

# Shallow geophysical evaluation of the transition zone between the Guaraní and Yrendá-Toba-Tarijeño aquifer systems (Argentine Gran Chaco)

Verónica Gisel Peri<sup>1,\*</sup>, Hernan Barcelona<sup>1</sup>, María Cristina Pomposiello<sup>1</sup>,  
Eduardo Antonio Rossello<sup>2</sup>, and Alicia Favetto<sup>1</sup>

<sup>1</sup>Instituto de Geocronología y Geología Isotópica, Pabellón INGEIS, Universidad de Buenos Aires, Consejo Nacional de Investigaciones Científicas y Técnicas. Ciudad Universitaria, C1428EHA - Ciudad de Buenos Aires, Argentina.

<sup>2</sup>Departamento de Geología, Facultad de Ciencias Exactas y Naturales, Pabellón 2, Universidad de Buenos Aires, Consejo Nacional de Investigaciones Científicas y Técnicas. Ciudad Universitaria, C1428EHA, Ciudad de Buenos Aires, Argentina.

\*gisel@ingeis.uba.ar; gisel\_peri@yahoo.com.ar

## ABSTRACT

The shallow geology and local hydrogeological systems of the Argentine Gran Chaco are poorly known. This area is part of the Chaco-Pampean Plain in the Andean foreland and is predominantly known by the subsurface data. Otumpa hills constitute a gentle topography located in the study area (26° - 28° S; 63° - 61° W) with N-S orientation. This morphology represents a transition zone between the western and eastern limits of the Guaraní and Yrendá-Toba-Tarijeño aquifer systems, respectively. Here, we report the results of two west-east profiles across Otumpa hills (northern profile at 26°40' S; southern profile at 27° S) consisting in vertical electrical soundings and audiomagnetotelluric soundings. We utilized 1-D and 2-D inversion techniques to obtain resistivity models from the measured data. The models defined several geoelectric layers, which were very consistent in both methods and in both profiles. We identified the upper geoelectric layer UL (> 20 Ωm), the semi-conductive geoelectric layers SC, SC<sub>2</sub> and SC<sub>3</sub> (6-20 Ωm), the conductive geoelectric layers C and C<sub>2</sub> (4-8 Ωm) and the highly conductive geoelectric layers HC and HC<sub>2</sub> (< 5 Ωm). SC and SC<sub>2</sub> showed the best hydrogeological possibilities of presenting freshwater. These layers lie on very porous aeolian sandstone and very silty loess. This is because they are hosted in the Pampa formation northward, in the Chaco formation southwestward, and in the Chaco or Tacuarembó formations eastward, which are laterally uplifted. The shallowest SC is 10 meters thick while SC<sub>2</sub> is 100 meters thick. Northward, SC<sub>2</sub> provides continuity to an analogous geoelectric layer identified eastward. Several boreholes corroborate the presence of freshwater at both levels. HC and C in the audiomagnetotelluric profiles and C<sub>2</sub> in the vertical electrical soundings profile suggest the presence of high-saline water (<8 Ωm). This 100-meter-thick hydrogeological level is the most exploited in the area and is hosted by the Pampa and Chaco formations. However, the saturated zone for all layers is unknown. HC<sub>2</sub>, the deepest hydrogeological level (between 250 and 350 meters), is hosted by the Chaco and Tacuarembó formations and could be related to the thermal high-saline water found southeastward at a depth of 350 meters depth. We correlated the shallowest levels (SC, SC<sub>2</sub>, HC, C and C<sub>2</sub>) with the Toba aquifer system that may pass eastward the Guaraní aquifer system because the Tacuarembó Formation is the host there and the deepest level HC<sub>2</sub> could also be related to the Guaraní aquifer system. The results provide a new shallow geological-geophysical

model of the Otumpa hills area that reveals aquifers more associated with lithology and topography than with stratigraphy. A slight ductile deformation is evidenced by the geometric shapes of HC<sub>2</sub> and SC<sub>2</sub> and by the gentle tilts that accompany the slopes (SC<sub>2</sub>, HC and SC). Finally, the relevance of this work resides in the local aquifers identification and providing information to improve its usually poor management in this region. Moreover, further studies are likely to provide new insights into the hydrological interaction between the Guaraní and Yrendá-Toba-Tarijeño aquifer systems of the South American region.

Key words: Guaraní aquifer system, Yrendá-Toba-Tarijeño aquifer system, Otumpa hills, audiomagnetotellurics, vertical electrical sounding, Gran Chaco, Argentina.

## RESUMEN

*El Gran Chaco Argentino forma parte de la Llanura Chacopampeana, en el antepaís andino, y es principalmente estudiado por información de subsuelo, aunque la geología somera y sistemas hidrogeológicos locales son poco conocidos. Las Lomadas de Otumpa, una topografía sutil N-S, ubicadas en este área (26° - 28° S; 63° - 61° W), representan una zona de transición entre los límites occidental y oriental de los Sistemas Acuíferos regionales Guaraní y Yrendá-Toba-Tarijeño, respectivamente. En este trabajo, se presentan los resultados de dos perfiles O-E (norte: 26°40' S y Sur: 27° S) a través de las Lomadas de Otumpa, obtenidos por sondeos eléctricos verticales y audiomagnetotellúrica. Las inversiones 1-D y 2-D realizadas permitieron definir capas geoeléctricas muy consistentes entre ambos métodos y perfiles. Se identificaron la capa geoeléctrica superior UL (> 20 Ωm), las capas geoeléctricas semi-conductivas SC, SC<sub>2</sub> y SC<sub>3</sub> (6-20 Ωm), las capas geoeléctricas conductivas C y C<sub>2</sub> (4-8 Ωm) y las capas geoeléctricas muy conductivas HC y HC<sub>2</sub> (< 5 Ωm). Las mayores posibilidades hidrogeológicas de contener agua dulce se presentan en SC y SC<sub>2</sub>. Estas capas consisten en loess muy limoso y arenisca eólica muy porosa que forman parte de la formación Pampa en el sector norte, de la formación Chaco al sudoeste y de las formaciones Chaco y Tacuarembó al este. La capa más superficial SC tiene 10 metros de espesor, mientras que SC<sub>2</sub> tiene 100 metros. Al norte, SC<sub>2</sub> otorga continuidad a una capa geoeléctrica análoga identificada al este. Varias perforaciones corroboran la presencia de agua dulce en estos niveles. HC y C en los perfiles*

audiomagnetotelúricos y  $C_2$  en los sondeos eléctricos verticales sugieren la presencia de agua con alto contenido salino ( $<8 \Omega m$ ). Este nivel tiene 100 metros de espesor, es el más explotado del área y se hospeda en las formaciones Pampa y Chaco. La zona saturada de cada nivel es desconocida. El nivel hidrogeológico más profundo  $HC_2$  (entre 250 y 350 metros), está hospedado en las formaciones Chaco y Tacuarembó y podría relacionarse al agua termal de alto contenido salino hallada al sudeste a 350 metros de profundidad. Los niveles más someros ( $SC$ ,  $SC_2$ ,  $HC$ ,  $C$  y  $C_2$ ) se correlacionaron al Sistema Acuífero Toba que hacia el este pasaría al Sistema Acuífero Guaraní, por hospedarse en la Formación Tacuarembó en ese sector. El nivel más profundo  $HC_2$  se correlacionó al Sistema Acuífero Guaraní. Los resultados introducen un nuevo modelo geológico-geofísico de las Lomas de Otumpa que revela niveles hidrogeológicos controlados por la topografía y litología más que por la estratigrafía. Una deformación dúctil incipiente se evidencia en las formas geométricas de  $HC_2$  y  $SC_2$  y en suaves inclinaciones ( $SC_2$ ,  $HC$  y  $SC$ ) que acompañan la topografía. Finalmente, el presente trabajo presenta relevancia para el conocimiento de los escasos recursos hídricos de esta región. Los resultados permiten definir los acuíferos locales y planificar su utilización. Regionalmente, podrá investigarse la interacción hidrológica entre los Sistemas Acuíferos Guaraní y Yrendá-Toba-Tarijeño de Sudamérica, aunque deben realizarse más estudios.

**Palabras clave:** sistema acuífero Guaraní, sistema acuífero Yrendá-Toba-Tarijeño, lomadas de Otumpa, audiomagnetotelúrica, sondeo eléctrico vertical, Gran Chaco, Argentina.

## INTRODUCTION

The shallow geology and local hydrogeological systems of the Argentine Gran Chaco are poorly known. This area is part of the Chaco-Pampean Plain (Chebli *et al.*, 1999) (Figure 1a), in the Andean foreland, and is characterized by tectonic stability and sedimentary aggradational processes that typify the intra-continental regions. This plain is predominantly known by the subsurface data. Particularly, Otumpa hills (Rossello and Bordarampé, 2005) (Figures 1b and 1c) constitute

a gentle topography located in this area ( $26^\circ - 28^\circ S$ ;  $63^\circ - 61^\circ W$ ) with N-S orientation. This morpho structure represents a transition zone between the main Guaraní and Yrendá-Toba-Tarijeño aquifer systems of the region (Figure 1a).

The stratigraphy, especially the first hundreds of meters of subsurface that involved mainly the Neogene period, is poorly understood. Most units are informally defined from regional correlations and from the significant association with geomorphological events. During the Quaternary, this region suffered several climatic changes that originated the observed landforms. In wet weathers, soils and elongate alluvial deposits were developed, whereas in semiarid weathers, alluvial megafans were developed by ephemeral courses, which originated areal sedimentation and alluvial flood. At extremely dry intervals, aeolian processes dominated and formed dune fields and loess mantles. These geomorphological units have interstratified aeolian and alluvial megafan deposits.

The thick Quaternary cover masks and rarely preserves the uplifted neotectonic structures. However, previous investigations have revealed that some of the topographic anomalies in this extensive plain may be related to neotectonic activity. In addition, a few reports have established that these neotectonic structures are associated with drainage system anomalies (Pasotti, 1968, 1974; Castellanos, 1968; Mon and Gutiérrez, 2009; Peri and Rossello, 2010). In the Argentine Gran Chaco, Otumpa constitute a positive morphologic structure that is related to blind inverse faults. The structure interrupts the plain and show paleo-drainage network anomalies of the North Salado River (Figure 1b).

On the other hand, the hydrogeological local systems are little known. Thus, obtaining water resources is basically a random event. The hydrogeological boreholes present in this area are destined to human consumption as well as for agricultural and cattle breeding, but the information is insufficient to characterize the circulation medium. However, the regional and transnational Guaraní aquifer system (GAS) is well known and Otumpa hills have been recently proposed as its western boundary (Peri, 2012; Rossello and Veroslavsky, 2012) (Figure 1a). Since this morphologic structure seems to control the disappearance of the main geological sequences that involved the GAS, Otumpa

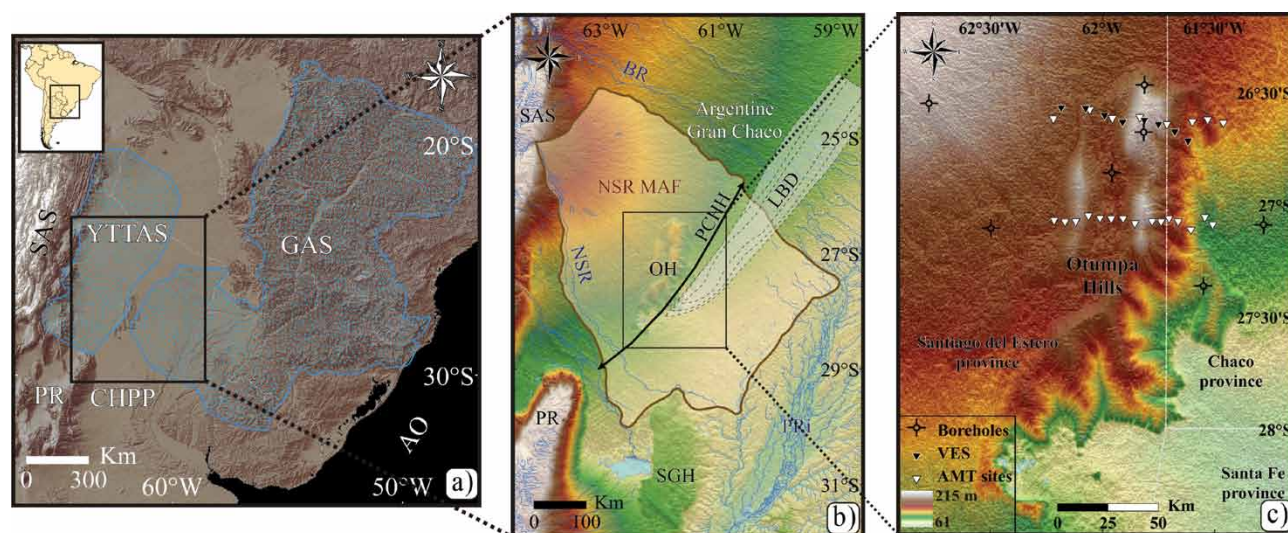


Figure 1. a) The main aquifer systems of the region (GAS: Guaraní aquifer system; YTTAS: Yendá-Toba-Tarijeño aquifer system) and some geotectonic features (CHPP: Chaco-Pampean Plain; PR: Pampean Ranges; SAS: Sub-Andean System; AO: Atlantic Ocean) are shown. b) A detail of the geotectonic and geomorphological features of the Chaco-Pampean Plain are shown (BR: Bermejo River; NSR: North Salado River; PRI: Paraná River; NSR MAF: North Salado River Mega-Alluvial Fan; LBD: Las Breñas Depocenter; PCHH: Pampeano-Chaqueño High; OH: Otumpa hills; SGH: San Guillermo High). c) The AMT sites and VES are presented.

hills has been suggested to form its natural limit. However, the western boundary of the GAS is difficult to define due to the scarce geological evidences. Also, the basement of Otumpa hills has been postulated as part of the eastern boundary of the transnational Yrendá-Toba-Tarijeño aquifer system (Figure 1a), which involves the water reservoirs that extend from the Sub-Andean piedmont to the Chaco-Pampean Plain (Baudino *et al.*, 2006).

Several works have demonstrated that the shallow geophysical methods constitute an effective technique to define different geoelectric layers for the first hundreds of meters of subsurface (Zonge and Hughes, 1988; Falgàs, 2007; Ramos-Leal *et al.*, 2007, among others). Then, it is possible to associate the data obtained to lithostratigraphic and hydrogeological features of the units known. The subsurface electrical resistivity is mainly dependent on the minerals and the fluid distribution, type and content, as well as on rock porosity and permeability and water saturation. The variation in the rock electrical resistivity, due to water content ranges around three orders of magnitude. Thus, since sediments with water have a higher conductivity than dry rocks, the electrical resistivity is an indicator of the presence of an aquifer.

The aim of our study was to evaluate the geoelectric properties of shallow sedimentary sequences and determine their hydrogeological possibilities beneath Otumpa hills. For this purpose, we applied the classical vertical electrical sounding (VES) (Orellana, 1972) and audiomagnetotelluric (AMT) (McNeill, 1990) methods. We report the results of eight VES across Otumpa hills in a W-E northern profile (26°S) and an AMT survey in two W-E profiles located at 26°S and 28°S (Figure 1c). Both geophysical data were processed to obtain 1-D inversion models and additionally, the AMT data were used to get 2-D inversion models, which provided an image of the electrical resistivity distribution in the subsurface. We correlated the geoelectric layers identified with the stratigraphy and lithology setting to obtain a shallow geological-geophysical model of the Otumpa hills area. Finally, we discuss the hydrogeological possibilities and compare both geophysical techniques.

## GEOLOGICAL SETTING

The study area is placed in the Chaco-Pampean Plain (central-north Argentina), which is part of the distal plain of the central Andean piedmont originated by the uplift and erosion of the Andean Cordillera (Figure 1a). This plain represents a largely aggradational environment (Chebli *et al.*, 1999; Iriondo, 1997) and is predominantly known by the subsurface data (mainly seismic and borehole data) of the petroleum exploration industry. In the study area, the crystalline basement was affected by an extensional tectonic event occurred at lower Paleozoic times, that originated Las Breñas hemigraben (Pezzi and Mozetic, 1989; Wiens, 1995) (Figure 1b). This depocenter is the main structural feature of the area and, is narrow and elongated by 250 kilometers in NE-SW direction. Its western border is abruptly marked by Las Breñas fault, which was partially tectonically inverted at Paleozoic times. This compressive tectonic event raised the Pampeano-Chaqueño basement high in the northwestern margin of Las Breñas depocenter (Chebli *et al.*, 1999) (Figure 1b) manifested on the surface as Otumpa hills (Rossello and Bordarampé, 2005) (Figures 1b and 1c). Otumpa hills are located between 26°-28°S and 63°- 61°W, with N-S orientation along 250 kilometers, and reaches 100 meters above the surrounding plain. We have previously interpreted this morphologic structure as a relict of Western Gondwana (Peri, 2012). Otumpa hills constitute a manifestation on the topography of preexisting blind faults that show seismic evidence of Mesozoic and Cenozoic tectonic reactivations. Also, shallow historic earthquakes occurring in the area (Volponi and

Aparicio, 1969) have revealed Quaternary movements.

<Otumpa hills are located within the North Salado River mega-fan (Iriondo, 1984, 1993), whose headwaters are in the Sub-Andean Ranges (Argentine northwest) and originally flowed to the SE by several hundreds of kilometers (currently do so in NNW-SSE direction), developing a dense network of paleo-channels (Figure 1b). Also, the extensive sand fields and loess mantles were originated by a great volume of silt and sand deflated in the Andean Cordillera during dry periods and transported to the distal plain. Both, aeolian and alluvial mega-fan deposits are interstratified. Additionally, a few quartzitic sandstone outcrops within silcrete levels crowned by a thin weathering profile are exposed in Otumpa hills (Batic *et al.*, 1995; Peri, 2012) (Figure 2). We have previously correlated these outcrops with aeolianite of Botucatu desert represented by the Tacuarembó Formation in this area (Bossi *et al.*, 1966; Russo *et al.*, 1979). The stratigraphic features of the area are summarized in Table 1. Figure 2 describes the lithology of some of the hydrogeological and petroleum boreholes of the study area.

Otumpa hills have been proposed as the western boundary of the regional and transnational Guaraní aquifer system (GAS) (Peri, 2012; Rossello and Veroslavsky, 2012) since the main geological sequences of this aquifer are absent to the west (Araújo *et al.*, 1995, 1999; Gastmans *et al.*, 2010, 2012; De Santa Ana *et al.*, 2008; among others) (Figure 1a). The outcrops in Otumpa hills related to the Tacuarembó Formation constitute important evidence. According to Araújo *et al.* (1995, 1999), the Triassic units: Botucatu Formation and Grupo Rosario do Sul in Brazil, the Buena Vista Formation in Uruguay and the upper Jurassic - lower Cretaceous Misiones or Tacuarembó Formation in Paraguay, Argentina and Uruguay, constitute the aquifer. Tacuarembó sandstone represents the main GAS reservoir that forms a thin and about continuous cover in the Paraná and Chaco-Pampean basins. The thickness average is 250 meters and is confined in 90% of its surface while the remaining 10% is free constituting the main direct recharge area.

The aquifer, in Chaco-Pampean and Paraná basins, is covered by the Serra Geral Basalt, which behave as an aquiclude-aquitard by fracturing, while in other areas such as the study area, it is covered by the Baurú, Mariano Boedo and Chaco formations (Vives *et al.*, 2001). In the study area, the GAS geometry is controlled by the reactivation of a system of faults and basement highs rather than by the thickness of Serra Geral Basalt, because it is absent. The recharge areas are in the topography highs and the discharge areas are associated with outcrop belts. In Argentina, due to the lack of water direct measures, some geoelectric profiles showing low electrical resistivity (<2 Ωm), have been used to infer that the water is possibly sodium chloride with a high mineralization (Gastmans *et al.*, 2012). Finally, in some areas of Argentina, Uruguay and Brazil, there are natural upwelling phenomena and low enthalpy geothermal resources with maximum water temperatures between 50° and 60 °C.

At the same time, the eastern boundary of the transnational Yrendá-Toba-Tarijeño aquifer system is located in Otumpa hills and involves the water reservoirs that extend from the Sub-Andean piedmont to the Chaco-Pampean Plain (Baudino *et al.*, 2006) (Figure 1a). The Toba aquifer system (TAS), located in the study area, is mainly characterized by two aquifer complexes: the Sub-Andean Tertiary Aquifer Complex, which is constituted by Tertiary sediments (Fuertes, 2004), and the Quaternary alluvial fan aquifers. The former is regional, developed in the Chaco formation, has variable hydrogeological characteristics and is located at different depths. The main recharge is allochthonous in the hydrological basins of the western mountains and water flux is controlled by the stratigraphy and the structure. The water reservoir has a quality ranging between good and acceptable, and the electrical conductivity is extremely variable.



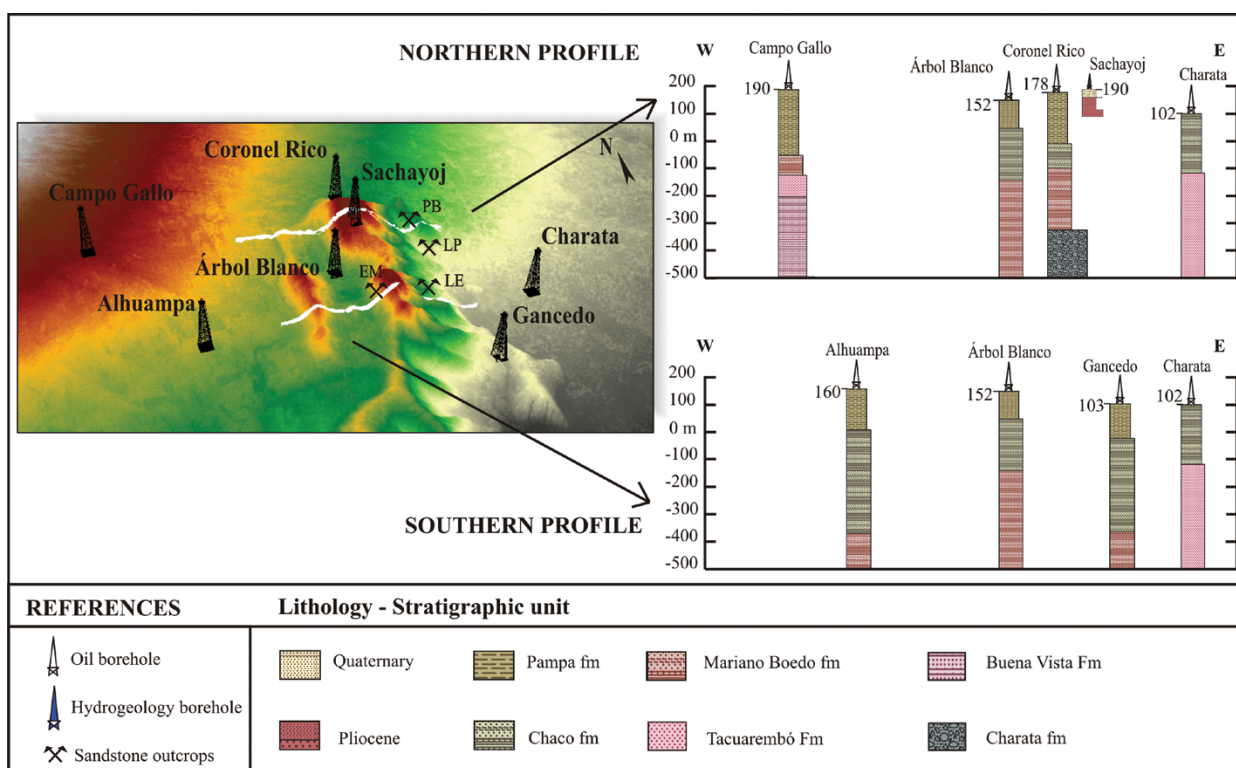


Figure 2. Hydrogeological and oil boreholes: Sachayoj N°1 (Dirección General de Minas y Geología, 1947), Alhuampa (Yacimientos Petrolíferos Fiscales YPF, 1966a), Árbol Blanco (YPF; 1966b), Campo Gallo (YPF, 1969a), Charata (YPF, 1943), Coronel Rico (YPF, 1969b), and Gancedo (YPF, 1970), and also Tacuarembó Formation outcrops are shown: Palo Blanco (PB), El Mercado (EM), Las Piedritas (LP), La Esperanza (LE). The lithostratigraphy of the boreholes for each profile is also plotted.

The Alluvial Fan Aquifer Complex is constituted by Quaternary sediments and involves the alluvial fans of the main rivers of the region as the North Salado. These deposits constitute the main reservoirs with sand and gravel sediments of the flood plain within paleo-channels. The thickness varies between 50 and 100 meters. In general, the fluvial courses have a strong influence on the groundwater flux of the shallow reservoirs while the deepest are more independent. These rivers represent the main recharge in the TAS by infiltration in their courses and their lateral movement into the Quaternary sediments.

The study area is characterized by the distal alluvial fan (Vargas, 1977; Angeleri, 2002) and has three regional aquifer levels. The shallowest reaches a depth of 30 meters and has a saline composition with freshwater lens, in saturated or partially saturated sands, sometimes dry sands. The second aquifer level is free or semi-confined, saline composition with freshwater levels and it is found at a depth of around 80 meters. The deepest aquifer level has freshwater, as well as water levels with very low salinities (0.5 mg/L), and have been detected in some deep boreholes (> 300 meters).

In contrast, the aquifer units in the study area are still unknown and the information is insufficient to characterize the circulation medium. Nevertheless, eastward of the study area, some shallow geophysical studies have been focused on localizing hydrogeological resources (Coriale, 2006; Rocha-Fasola *et al.*, 2009) and gravel for road construction (Bonini, 1980). These reports have shown a common medium-resistive layer (20 to 40  $\Omega$ m) with hydrogeological possibilities of freshwater between 50 and 100 meters depth. Deeper, a very conductive zone (1 to 5  $\Omega$ m) carries highly saline water and is probably related to the level most exploited in the area. Finally, a thermal aquifer composed of hyper-saline water and with 40 °C lies around 350 meters depth (Coriale, 2006).

## GEOPHYSICAL EVALUATION

### Audiomagnetotelluric data

#### Theory

The magnetotelluric method (MT) explores the distribution of electrical conductivity within the Earth. An MT sounding measures time-varying electric and magnetic fields, simultaneously. The external magnetic field has a natural source, which is mainly constituted by global electric storms (lightning discharges) and solar activity (Earth's magnetosphere and ionosphere and solar wind interaction). The variations in the magnetic field induce the electric and secondary magnetic fields, which are not independent. The audiomagnetotellurics (AMT), which is an extension of the MT method that uses a higher frequency range (1 Hz to 1 MHz), is useful to investigate the first hundreds of meters beneath the surface (McNeill, 1990). An AMT sounding records the horizontal components of the magnetic ( $H_x$ ,  $H_y$ ) and electric fields ( $E_x$ ,  $E_y$ ), where  $x$  and  $y$  constitute horizontal and orthogonal directions. Using the Fourier-Transform, the time-series obtained are converted into the frequency domain, where the horizontal field components are related by a complex  $2 \times 2$  MT impedance tensor,  $Z$  (Vozzoff, 1972; Kaufman and Keller, 1981; Simpson and Bahr, 2005):

$$\begin{aligned} E_x &= Z_{xx} H_x + Z_{xy} H_y \\ E_y &= Z_{yx} H_x + Z_{yy} H_y \end{aligned} \quad (1)$$

$Z$  depends on the subsurface conductivity; thus, its calculation in a frequency range allows obtaining the electrical structure of the Earth's subsurface.  $Z$  is complex, being composed of both real ( $Re$ ) and imaginary ( $Im$ ) parts. So, the components of  $Z$  allow defining the apparent

Table 1. Stratigraphic features of the area.

Era	System Period	Series Epoch	Russo <i>et al.</i> (1979)	Iriondo (1990)	Marengo (2006)	Lithology	Thickness (m)	Depositional environment	
Cenozoic	Quaternary	Upper Holocene	Pampa fm	Sand fields	Littoral gp. Chaco fm. (undifferentiated)	Sand fields and silt layer	0.20-0.30	Semi-arid period originated little sand fields (Iriondo, 1990).	
		Middle Holocene		Pedogenetic layer		Pedogenetic layer (8,500-3,500 y B.P.) (Iriondo and García, 1993)			
		Upper Pleistocene		Urundel Fm		Illitic and quartzite dominant loess unit. Volcanic glass absent. Eolian system interstratified with alluvial sediments of the North Salado system 16,900 y B.P. (Iriondo, 1990). It is Chaqueño loess, secondary and reworked with sub-tropical features (Sayago <i>et al.</i> , 2001).	18	Periglacial and glacial processes during the Last Glaciation Maximum.	
	Neogene	Quaternary <i>s.l.</i> -Pliocene	Chaco fm	Western Alluvial Mega-fans		Alluvial deposits conformed by loessic sediments and paleo-channels. Composition is predominantly silt, fine sand and clay (+ 90 % illite) (Iriondo, 1990). The chlorides are predominant between the soluble salts, followed by sulphates and carbonates (Iriondo and Bautista, 2008).	120	The major fluvial courses of the western area developed these alluvial fans (Pliocene-present), with interruptions during dry extreme or very humid periods.	
			Upper Miocene						
			Oligocene						
Mesozoic	Upper Cretaceous	Eocene							
		Paleocene	Mariano Boedo fm			Sandstones with pelitic and limestone intercalation to the top. At bottom should present a conglomerate with basalt clasts. Westwards it is mainly composed of fine to medium grain size with scarce matrix. Gray, greenish, pink clays are found in less proportion and crystalline and muddy gypsum levels. Fine to medium consolidated sandstone. The mainly component is quartz generally very well rounded. The stratification has variable scale with eolian cross-bedding. Laminar reddish lutites are intercalated. They are mainly yellowish gray to gray pink. In other areas, they are interdigitated with Serra Geral basalts (Bossi, 1966; Scherer, 2002).	300-500	Continental to coastal marine transition environment (Padula and Mingramm, 1963; Russo <i>et al.</i> , 1979).	
	Lower Cretaceous	Tacuarembó Fm							
		Upper Jurassic							
Paleozoic	Permian-Carboniferous	Charata fm				Mainly diamicritic composition with very angular quartzite, black lutites and metamorphic clasts in a silt-clayey matrix. Sandy intercalations are common at bottom and black lutites intercalations are present at succession top.	200-600	Glacial	

resistivity ( $\rho$ ) and the phase ( $\varphi$ ) as a function of period (or frequency  $\omega$ ):

$$\rho_{ij}(\omega) = \frac{1}{\omega\mu} |Z_{ij}(\omega)|^2 \quad (2)$$

$$\varphi_{ij}(\omega) = \frac{1}{\omega\mu} \frac{\text{Im}(Z_{ij}(\omega))}{\text{Re}(Z_{ij}(\omega))} \quad (3)$$

where  $\mu$  is the magnetic permeability of free space.

In a 1-D layered Earth, the conductivity varies only with depth, the diagonal components of  $Z$  are zero, and the off-diagonal elements are equal in magnitude but have opposite sign. In a 2-D medium, the conductivity parallel to the structural strike is constant and varies with both the direction perpendicular to strike and the depth, the diagonal components of  $Z$  are equal to zero, and the off-diagonal elements differ in magnitude and have opposite signs. A rotation of the coordinate system allows finding two orthogonal directions in which the diagonal components of  $Z$  are zero. In the real world, a close-to 2D geologic situation leads to find a direction that coincides with the geological structure, which is denominated as geoelectric strike. In this case, data can be separated into two independent polarization modes, one with electrical current flowing parallel (transverse electric polarization) and other perpendicular (transverse magnetic polarization) to the strike direction (Vozzoff, 1972; Kaufman and Keller, 1981). In a general case it is not possible to find a direction in which the diagonal components of  $Z$  become zero, because of the presence of distortion or due to 3-D induction (or both). The depth of penetration of the electromagnetic field (skin depth) depends on the electrical resistivity of the Earth and of the signal period (Simpson and Bahr, 2005). An increase in medium resistivity implies an increase in the signal penetration. On the other hand, high frequency signals are attenuated close to the surface, while longer periods reach deeper penetrations.

#### Sounding setting, data acquisition and processing

The sites arrangement during the AMT survey was selected according to available geological, hydrogeological and borehole data and supported by morphostructural analysis. A total of 23 AMT sites were collected along two W-E profiles 80 km long that crossed Otumpa hills (Figure 1c). The southern profile, located around 27°S, consisted of 15 AMT sites five kilometers equidistant. First, we measured the southern profile with 10 kilometers equidistance and then added AMT sites between them to decrease the equidistance to five kilometers. Since the results for both equidistances were similar (probably related to the homogeneous geological and hydrogeological features), we decide to measure sites separated 10 kilometers for the northern profile located around 26°40'S and constituted by eight AMT sites.

The final penetration depth reached for both models was around 400 meters with 5,000 or 10,000 meters equidistance between the AMT sites. This arrangement produces a too smaller lateral resolution in comparison with the depth resolution. The minor lateral resolution should be theoretically compensated by the homogeneity of the sedimentological layers and environment. However, we have considered the potential effects caused by the different resolutions in the interpretations of the 1D and 2D inversion models.

We used the Geometrics STRATAGEM equipment during the survey with classical field configuration. Two 50-meter-long orthogonal dipoles with steel electrodes oriented N-S and E-W were used to measure the horizontal electric field and two BF6 induction coils were used to measure the horizontal magnetic field. After some field tests, we decided to span the frequency range from 10 Hz to 1,000 Hz to enhance the productivity time and avoid noisy signals derived from higher frequencies without controlled source antenna.

The Geometrics Imagem software was used to control the recording, pre-processing and processing of the data. The receiver records the magnetic and electric signals that are pre-amplified and filtered. Also, manual gain setting for each channel, calculation of the complex impedance tensor  $Z$ , resolution of transfer functions and acquisition of values for apparent resistivity and phase of the signal were systematically carried out in the field. More than thirty coherent time-series segments were recorded for each site and were stacked for robust analysis to reduce the effects of bias because of noise. We tested several values of coherency threshold for apparent resistivity and phase and finally used 0.8 for both, which allowed us to obtain high quality data.

#### Distortion, dimensionality and strike analysis

AMT dimensionality and distortion were estimated using the skew approach, which is based on the  $Z$  magnitude asymmetry. Swift (1967) defined the  $skew_{Swift}$ , the most common asymmetry parameter, as the ratio module between the trace and the off-diagonal difference of the impedance tensor. An undifferentiated 1-D/2-D medium response may be assumed with a  $skew_{Swift}$  close to zero, while 3-D local anomaly is assumed when the value is greater than 0.2 (Bahr, 1991; Reddy *et al.*, 1977). Another asymmetry parameter is the phase-sensitive skew ( $skew_{Bahr}$ ), defined by Bahr (1988) as the normalized measure of the phase difference between each pair of tensor elements. This asymmetry parameter uses the phase signal with the advantage of being less sensitive to some particular source of distortion. It is commonly accepted that a value above 0.3 indicates 3-D data (Bahr, 1991). We used both skews and required them to be zero in order to suppose a 2-D medium mainly in areas with low galvanic distortion as this case (Berdichevsky and Dmitriev, 2008). Figure 3 shows the values of  $skew_{Swift}$  and  $skew_{Bahr}$  for each site at all frequencies for the northern and southern profiles. This figure evidences a few values slightly above the threshold but without any preferential frequency distribution. Therefore, skew parameters analysis suggests no significant distortion over the signal and that the general assumption of the 2-D medium may be valid for low noise level.

From a geo-structural point of view, the study area corresponds to a 1-D medium where the variations are controlled by the stratigraphic and hydrogeological horizons, all partially subordinate by the mainly N-S morphostructural trend of Otumpa hills. In this case, the probable geoelectric strike direction is N-S. However, a geophysical approach to the dimensionality of the signal is needed to confirm this assumption. Principal component axes rotation of the  $Z$  tensor, singular value decomposition (LaTorraca *et al.*, 1986) and local-regional tensor decomposition (Groom and Bailey, 1989) were carried out to define the geoelectric strikes. The three methods showed similar results probably due to the quality of the signal. Nevertheless, the local-regional tensor decomposition may not be significantly effective since the skin depth related to the two decades used in this study is low to accept a regional 2-D control over the signal, as demonstrated by Berdichevsky and Dmitriev (2008). Therefore, we used the resulting curves after the principal axes rotations, taking into account the low distortion of the signal determined.

#### 1-D inversion model

The invariant curves for resistivity and phase were used to calculate the 1-D inversion for each AMT site (Figure 4). Both electric and magnetic transverse polarizations were used to calculate the resistivity and phase invariants, which result from the geometric mean of the apparent resistivity and the arithmetic mean of the phases, respectively. Bostick and Occam algorithms were used to obtain an inversion approach and to determine the minimum number of layers with good fit to the data (Constable *et al.*, 1987). Generally, a five-layer model, which included

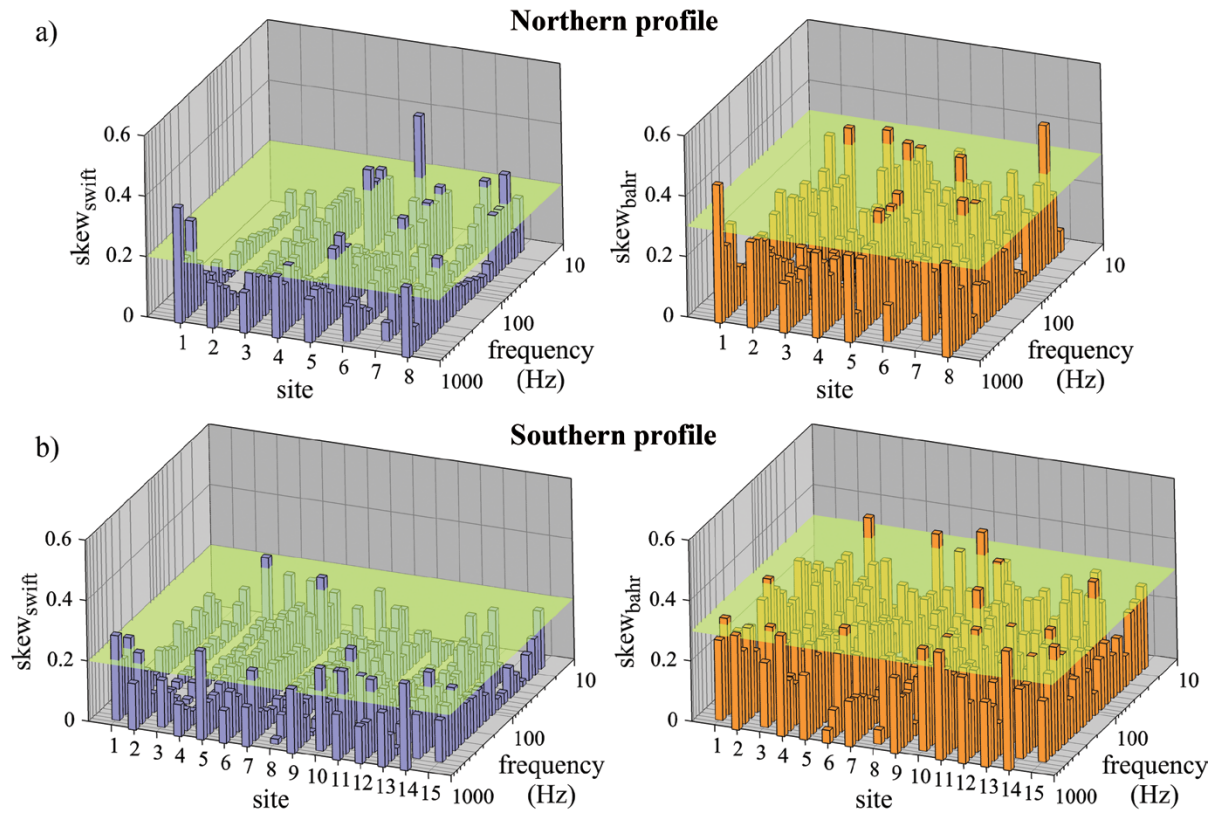


Figure 3. Frequency distributions of  $Skew_{Swift}$  and  $Skew_{Bahr}$  for all sites at all frequencies are shown. Dimensionality thresholds are represented by a green layer.

the lower half-space, was enough to fit the model response with the data curves measured at each site. From 1-D models, we observed that the ground resistivity values are less than  $50 \Omega \text{ m}$  and that when the conductivity decreases with depth, it does gradually. In several AMT sites, some layers were more resistive than the rest. This observation was then analyzed in the 2-D models.

#### 2-D inversion model

The 2-D inversion of the AMT data was carried out with the non-linear conjugate gradient algorithm of Rodi and Mackie (2001) available in WinGLink software. The starting models were made over four different meshes for each profile (Figure 5a). Each AMT site was centered in columns with a regular arrangement in all the profile and the rows were added at depth with a logarithmic spacing. The shallowest row calculated was 1.5 meters thick for the southern profile and 2.6 meters thick for the northern profile. The total depth of the grid reached approximately 3,000 meters. The different initial meshes were assigned a resistivity of 50 or  $100 \Omega \text{ m}$  to the entire mesh. Also, was considered the topographic influence in each case. The best results were obtained by the meshes with a background of the resistivity values of  $50 \Omega \text{ m}$  and those that did not include the topography because of the plainness of the area. Finally, the inversion parameter values were modified to analyze different responses and results. The roughness model was minimized through the iterative algorithm towards a pre-established misfit. Several inversions were done to achieve the most reliable models. These inversions allow varying the resistivity and testing the transverse electrical and magnetic polarizations independently and the transverse electrical and magnetic polarizations together. The complete frequency range was used between 10 Hz and 1,000 Hz. The final models selected (Figure 5b) had the most reliable features expected by the geological data and the parameters calculated

previously. The smoothness parameter  $\Upsilon$  had a value equal to three in the final models. The resistivity error floors were 10% and phase error floors were  $2.87^\circ$ , thus assigning a higher weight to phases in order to overcome the static shift problem. These models presented a good inversion misfit with a normalized root means square (NRMS) of 1.295 and 1.644 for the southern and northern profiles, respectively. To remark this good inversion misfit the frequency distribution of the NRMSs obtained in the 2-D inversion models for each AMT site is shown in Figure 6. The models presented were smoothed interpolating by kriging and the resistivity scales were logarithmic. This smoothed has maintained the same model and was only done to improve its graphic presentation. The skin depth reached for both models is around 400 meters due the highly conductive nature of the medium.

#### Geoelectric layers

The final models (Figures 5b and 5c) allowed us to identify several geoelectric layers in each of the profiles measured (Figure 5d).

#### Southern profile

The upper geoelectric layer (UL) is characterized by apparent resistivity values greater than  $20 \Omega \text{ m}$ . It is the shallowest geoelectric layer with a thickness of 20 meters and a horizontal disposition along the entire profile.

The semi-conductive (SC) geoelectric layer is characterized by apparent resistivity values between 6 and  $20 \Omega \text{ m}$ . This geoelectric layer underlies UL and is 10 to 20 meters thick, with horizontal disposition along the entire profile. The geoelectric layer  $SC_2$ , which has similar characteristics, is observed deeper, with lenticular geometry and a thickness of 40 to 80 meters that increases between AMT sites 4 and 9 and to the east of AMT site 11. Finally, a geoelectric layer  $SC_3$



is observed beneath 350 meters depth, but the model is inaccurate at those depths. The presence of SC, SC<sub>2</sub> and SC<sub>3</sub> was also detected by the 1-D models of the AMT sites 4, 5, 6, 7, 8, 9, 13, 14 and 15 (Figure 4) that showed thicker resistive layers than the rest of the AMT sites.

The highly conductive (HC) geoelectric layer is characterized by apparent resistivity values lower than 5 Ωm. This geoelectric layer underlies SC and is around 50 meters thick, with horizontal disposition along the entire profile. The geoelectric layer HC<sub>2</sub>, which has similar characteristics, is observed beneath 200 meters depth and is 100 to 150 meters thick. The geoelectric layer HC<sub>2</sub> is slightly heterogeneous, with lenticular geometry that becomes thinner at the center of the profile and thicker between AMT sites 1 and 4 and between AMT sites 9 and 12.

The conductive (C) geoelectric layer is characterized by apparent resistivity values between 5 and 8 Ωm. This geoelectric layer underlies HC and is around 20 meters thick, with horizontal disposition along the entire profile. The geoelectric layer C<sub>2</sub>, which has similar characteristics, is observed deeper, beneath SC<sub>2</sub>, and is 50 meters thick, with undulating topography. Finally, beneath HC<sub>2</sub>, the geoelectric layer C<sub>3</sub>, which is around 40 meters thick, shows horizontal disposition along the entire profile.

*Northern profile*

The upper geoelectric layer (UL) is characterized by apparent resistivity values greater than 20 Ωm (Figure 5c). It is the shallowest

layer, with a thickness of 6 to 8 meters, and is observed at the west side of the profile.

The semi-conductive (SC) geoelectric layer is characterized by apparent resistivity values between 6 and 20 Ωm. SC underlies UL and is 10 to 15 meters thick, slightly tilted to the west from the center of the profile. The deeper geoelectric layer SC<sub>2</sub> is 50 to 100 meters thick, with lenticular geometry that becomes thinner to the extremes of the profile and thicker between AMT sites 4 and 8. Finally, a geoelectric layer SC<sub>3</sub> is observed beneath 350 meters depth, but the model is inaccurate at those depths. The presence of SC, SC<sub>2</sub> and SC<sub>3</sub> was also detected by the 1-D models of the AMT sites 5 and 6 (Figure 4) that showed thicker resistive layers than the rest of the AMT sites.

The highly conductive (HC) geoelectric layer is characterized by apparent resistivity values lower than 5 Ωm. HC underlies SC and shows lenticular geometry that becomes thinner to the east of AMT site 4 and thicker to the west extreme of the profile. At the western side of the model, it reaches 100 meters thick, while to the east it decreases to around 50 meters. Also, it is slightly tilted to the west from the center of the profile. The geoelectric layer HC<sub>2</sub>, which has similar characteristics, is observed beneath 150 meters depth, with a thickness of 200 meters that decreases to the west to around 100 meters, acquiring lenticular geometry, and horizontal disposition to the east.

The conductive (C) geoelectric layer is characterized by apparent resistivity values between 5 and 8 Ωm. C and C<sub>2</sub>, which have the same

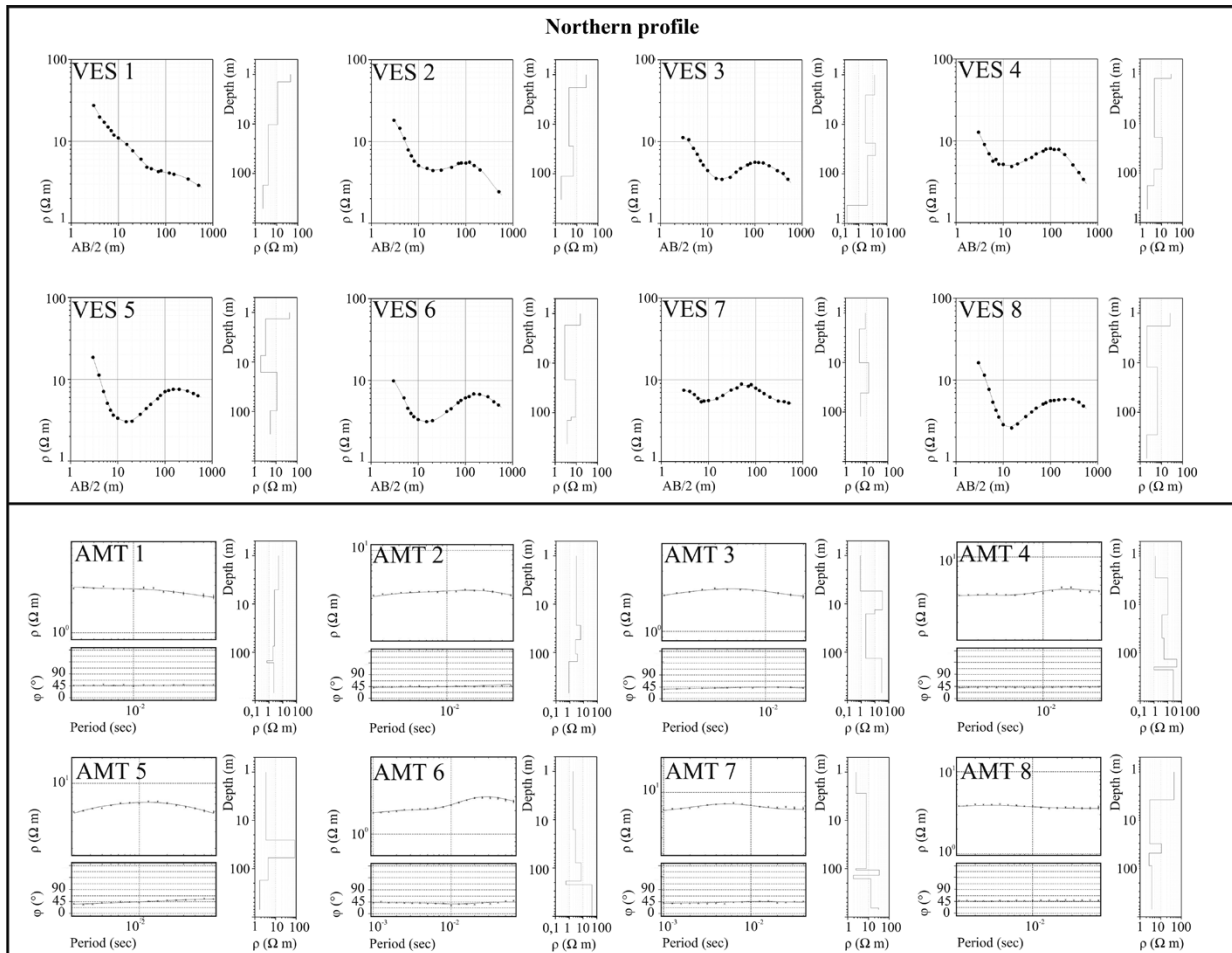


Figure 4. The invariant curves for resistivity and phase and the layer models obtained from the 1-D inversion are shown for each AMT site and correspond to the northern and southern profiles. The curves measured and the layer models obtained from all VES are also shown for the northern profile. (continues).



characteristics, lie below and above HC<sub>2</sub>, respectively. These layers are around 20 meters thick and accompany the geometry of HC<sub>2</sub>.

**Vertical electrical sounding method**

*Theory*

The main aim of a vertical electrical sounding (VES) is to obtain the vertical distribution of apparent resistivity with depth in the site of measurement. A VES is very useful to detect and establish the horizontal boundaries of a stratified subsurface. A VES consists in injecting electric current to the subsurface through a pair of steel electrodes usually called current electrodes (AB) and measuring the potential electric difference through a pair of copper electrodes (MN), which are in line with AB. There are several electrode arrangements such as Schlumberger, Wegener, among others, that reach different aims and depths (Orellana, 1972). The electric current penetration depth depends on the separation of the AB electrodes as well as of the electrical stratigraphy. If the distance between AB increases, the current flows deeper but its density decreases. In an isotropic and homogeneous medium 50% of the current flows above AB/2 (Orellana, 1972). However, it is not possible to fix a depth limit beneath the surface that does not influence VES, because the current density decreases slightly and gradually and we can assume that it is proportional to AB.

However, this idea is valid for a homogenous and isotropic subsurface, which, in general, does not exist.

The apparent resistivity  $\rho_{ap}$  is calculated with the current electric values measured ( $I$ ) in milliamperes and with the potential difference ( $\Delta V$ ) in millivolts as follows:

$$\rho_{ap} = K (\Delta V)/I \tag{4}$$

where  $K$  is the geometric factor that only depends on the geometric arrangement of electrodes (Orellana, 1972).  $\rho_{ap}$  represents an unreal earth resistivity, except in a homogeneous and isotropic medium, where this expression coincides with the real resistivity of the medium. The  $\rho_{ap}$  variation versus the current electrode semi-distances (AB/2) is plotted in logarithmic scales for each VES. Finally, the apparent resistivity of experimental data is inverted to obtain 1-D models of the ground resistivity, models of stratified layers, whose responses fit the experimental curve, minimizing the RMS. Commonly, since experimental curves admit several solutions, we must choose the most geological and reliable 1-D model. The geological information reduces, although it does not remove entirely, the ambiguity between 1-D models (Orellana, 1972).

*Sounding setting, data acquisition and processing*

VES were measured in eight sites, through a WNW-ESE profile (~ 26°30'S) that crosses Otumpa hills along 70 kilometers (Figure 1c)

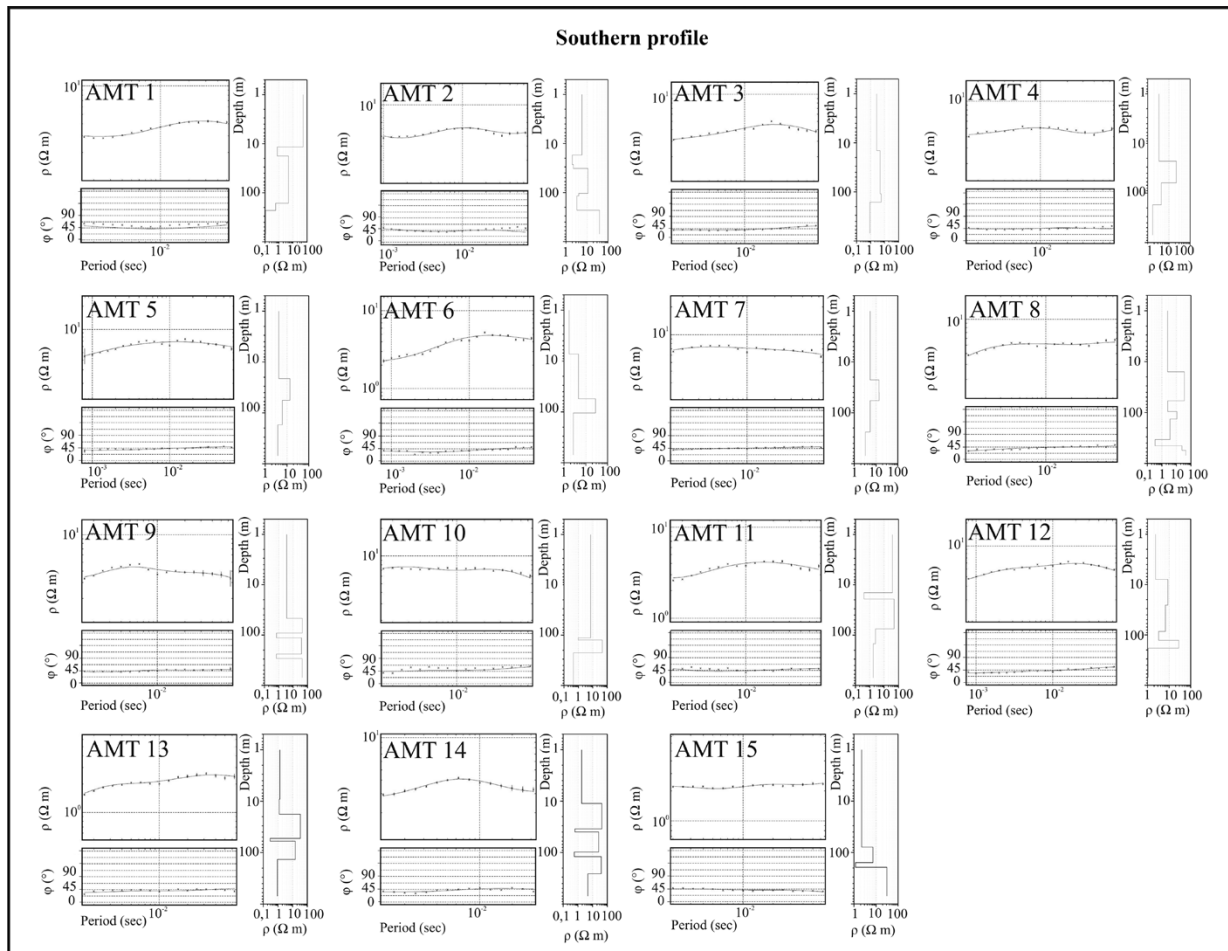


Figure 4 (continued).

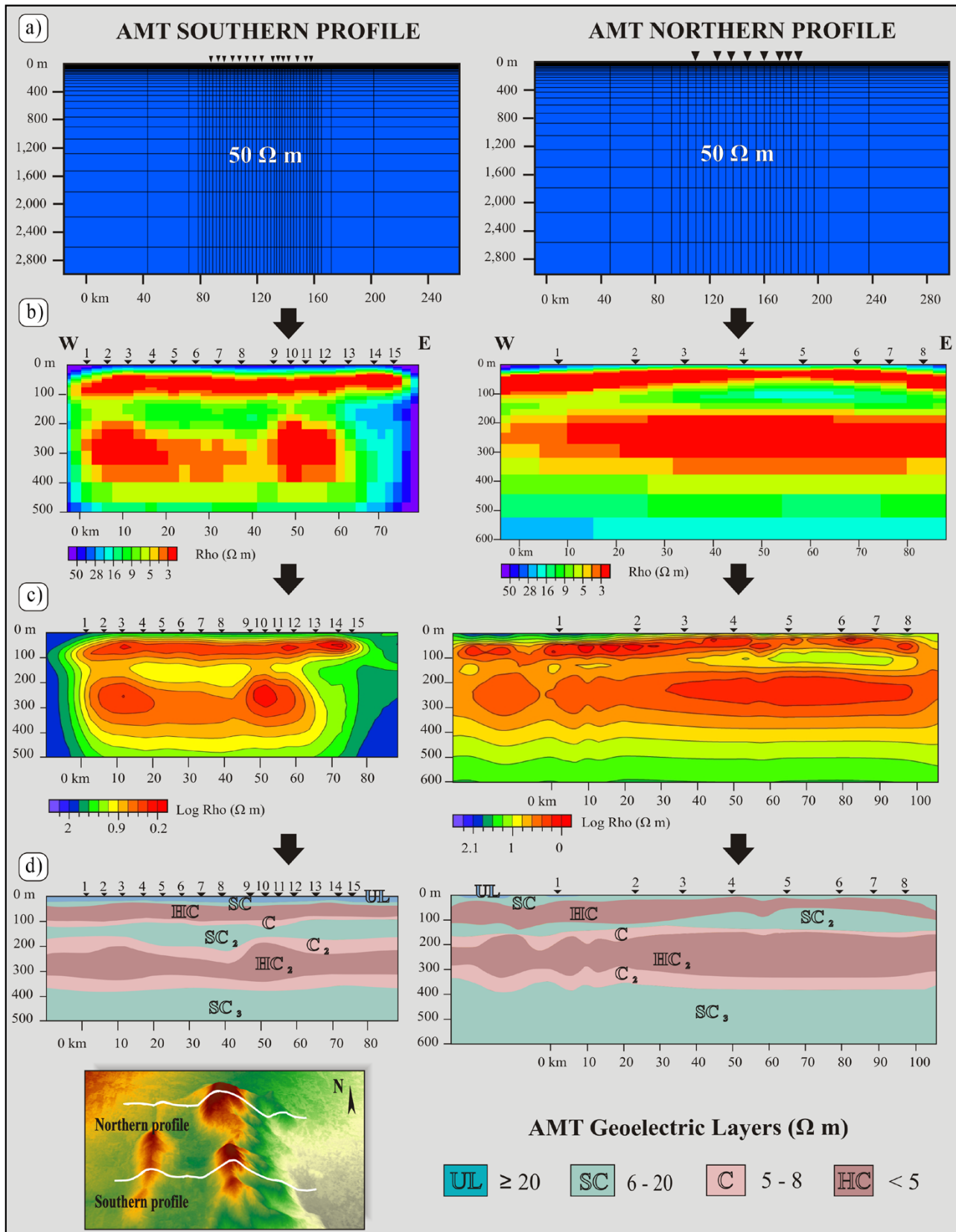


Figure 5. a) The starting meshes for the AMT 2-D inversion models are shown for the northern and southern profiles. b) The final AMT 2-D inversion models obtained are shown. c) The same models were smoothed interpolating by kriging. d) The interpretation of the geoelectric layers of the 2-D inversion models are also presented at a depth of 600 meters (UL: Upper geoelectric layer, SC: semi-conductive geoelectric layer, C: Conductive geoelectric layer, HC: Highly conductive geoelectric layer).

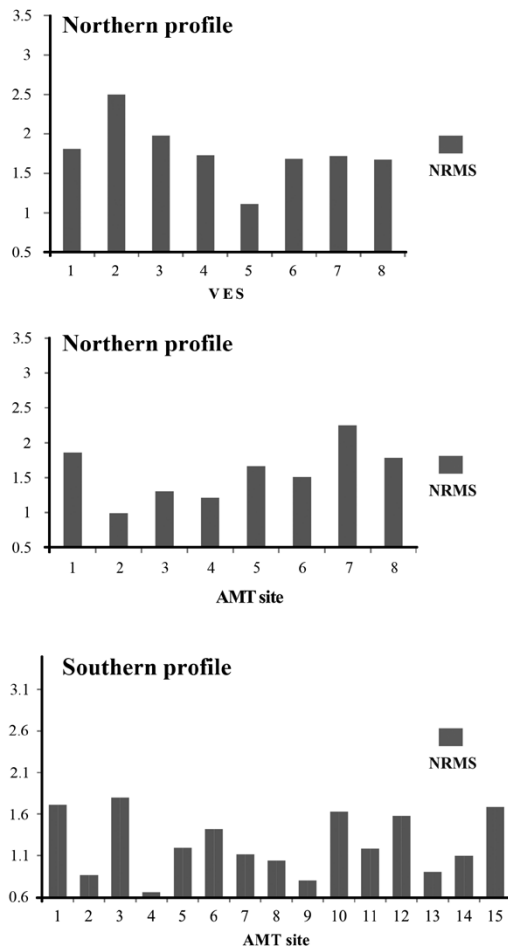


Figure 6. The frequency distribution of the NRMSs obtained in the 2-D inversion models for each AMT site and in the 1-D models for each VES are plotted.

and had almost the same trace as that of the AMT northern profile, with six to eight kilometers VES equidistance. The VES were measured with non-commercial equipment constructed with a current resource connected to a 1,000 watt generator that allowed obtaining intensities of up to 1 Ampere. The A and B current electrodes were of steel and the M and N electrodes were of copper to avoid the polarization between them. The current and electric potential were measured with very accurate ammeter and voltmeter. We used the Schlumberger arrangement, which uses a shorter distance between M and N than between A and B. The measures consist in expanding the distance between A and B in a regular way along the profile until it allows reaching the desired exploration depth. We increased AB/2 until reaching an opening of 500 meters to reach a good depth penetration although it also depends of the electric stratigraphy. We carried out three to five measures in each site. Since they showed regular and good quality values with exceptional anomalies, we averaged the data per site discarding every anomaly observed.

**1-D inversion model**

The 1-D inversion of the VES data was carried out with the IPI2win software (Bobachev et al., 2011). First, we obtained the  $\rho_{ap}$  calculated variation versus the current electrode semi-distances (AB/2) in logarithmic scales for each VES. Then, from the  $\rho_{ap}$  calculated, we modeled the 1-D inversion that results in a layer model for each VES (Figure 4). The 1-D model inversion of the electrical resistivity fit the experi-

mental curves. These models presented a good inversion misfit and a frequency distribution of the NRMSs obtained in each VES is shown in Figure 6. Figure 4 shows the experimental curves and the 1-D inversion model obtained for each VES. Although the experimental conditions provided good-quality data, we considered that this method provides different models from similar experimental curves. Our values were very consistent, which notably reduced the variety of possible models. The maximum depth reached was approximately 500 meters.

**Geoelectric layers**

The final 1-D models (Figure 7) allowed us to identify several geoelectric layers that were separated in four groups by their electrical resistivity values.

The upper geoelectric layer (UL) is characterized by apparent resistivity values greater than 20  $\Omega m$ . It is the shallowest layer, with a thickness of one to two meters and a discontinuous disposition.

The semi-conductive (SC) geoelectric layer is characterized by apparent resistivity values between 8 and 20  $\Omega m$ . SC underlies UL or lies on the surface, is one to ten meters thick, and shows a discontinuous disposition. SC<sub>2</sub>, which has similar characteristics, is deeper, and is 20 to 100 meters thick. SC<sub>2</sub> shows lenticular geometry, becoming thicker at the center of the profile between VES 4 and 7 and thinner at the extremes of the profile.

The conductive (C) geoelectric layer is characterized by apparent resistivity values between 4 and 8  $\Omega m$ . This layer underlies UL or SC and sometimes lies on the surface, and is 10 to 20 meters thick. C<sub>2</sub>, which has similar characteristics, is observed deeper, mainly beneath SC<sub>2</sub>, and is between 100 and 400 meters thick. C<sub>2</sub> shows lenticular geometry, being thickest in VES 3, 5 and 8.

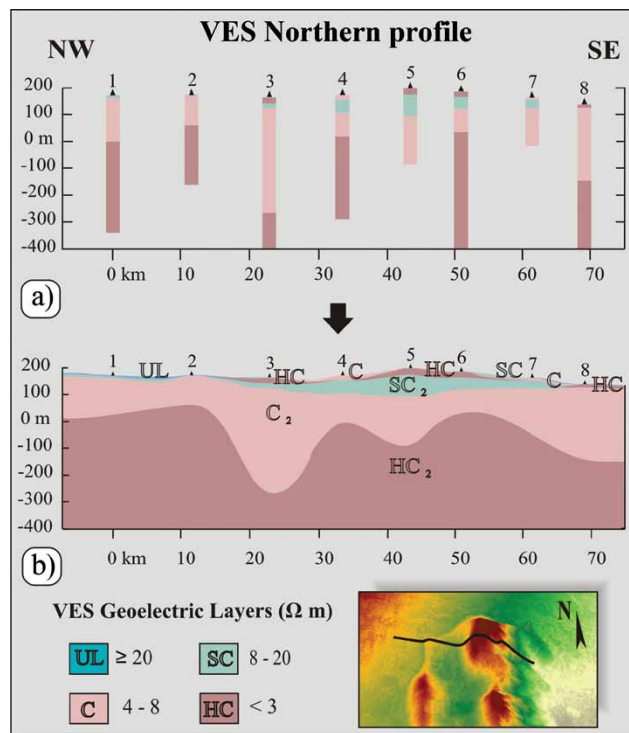


Figure 7. a) The 1-D layer models of the VES profile are shown. b) The 2-D interpretation with geoelectric layers identified is presented (UL: Upper geoelectric layer, SC: Semi-conductive geoelectric layer, SC<sub>2</sub>: Deeper semi-conductive geoelectric layer, C: Conductive geoelectric layer, C<sub>2</sub>: Deeper conductive geoelectric layer, HC: Highly conductive geoelectric layer, HC<sub>2</sub>: Deeper highly conductive geoelectric layer).





Table 2. Correlations and properties of the identified aquifers. In the column of lithostratigraphic units, is also denote the area where they appear (North, South or East). In the column of depth, the depth levels of the geoelectric layers in the water boreholes (boreholes), in a geophysical profile specific (AMT north, south or VES) or in all the geophysical profiles (geophysics) are shown. In the column of thick values, the observed average thick values are shown. In the column of Aquifer system, the aquifer system associated is indicated (East: East area). TAS: Toba aquifer system, AFAC: Alluvial Fan Aquifer Complex, GAS: Guaraní aquifer system.

Geoelectric layers ( $\Omega$ m)		Lithostratigraphic units	Depth (meters)	Thickness (meters)	Aquifer system	Water quality
VES	AMT					
	UL $\geq$ 20	Pampa fm.		~ 5-20		
	SC: 6 - 20	Pampa fm.	1-15 (boreholes)	10	TAS (AFAC) East: GAS	Freshwater
C <sub>2</sub> : 4 - 8	C: 4 - 8	North: Pampa and Chaco fms. South: Pampa fm. East: Tacuarembó Fm.	80 - 180 (boreholes) 50 - 200 (geophysics)	100	TAS (AFAC) East: GAS	High-saline water
	HC <sub>2</sub> < 5					
	SC <sub>2</sub> : 6 - 20	North: Pampa fm. South: Chaco fm. East: Tacuarembó Fm.	10-70 (boreholes) 20-100 (VES) 40-150 (AMT north) 80-150 (AMT south)	100	TAS (AFAC) East: GAS	Freshwater
	HC <sub>2</sub> < 5	Chaco and Tacuarembó fms. (subordinate Mariano Boedo fm.)	250-350 (geophysics)	~ 100	GAS	High-saline thermal water

profile. However, the Chaco and Mariano Boedo formations still show correlations with the same conductive geoelectric layers HC<sub>2</sub>, C and C<sub>2</sub> (Campo Gallo, Árbol Blanco, Coronel Rico and Charata boreholes). In the southern AMT profile, the Chaco formation becomes thicker in the low topography areas outside Otumpa hills (Alhuampa and Gancedo boreholes) and is observed in a higher level between the hills (Árbol Blanco borehole), which coincides with the maximum thickness of SC<sub>2</sub>. So, the Chaco formation is related to SC<sub>2</sub> in the southern profile.

Although there is not direct superposition of the Tacuarembó Formation with SC<sub>2</sub>, we are also correlated both north and south of the study area and is mainly constrained to its eastern part, which is corroborated by two important evidences. First, the location of the Palo Blanco (between AMT sites 6 and 7), Las Piedritas and La Esperanza quarries appears on the oriental slope of the most eastern Otumpa hills. Second, stratigraphic differences are observed between the eastern Charata borehole, which shows Tacuarembó Formation register in depth, and the western Alhuampa borehole, which shows the absent of this unit (see Figure 8). Chaco and Mariano Boedo formations pass the Tacuarembó Formation laterally from the west to the east. Besides, some additional data from the southern of Otumpa hills provides information about this transition style. For instance, although in El Mercado quarry outcrops the Tacuarembó Formation, the nearest borehole description (*i.e.*, Árbol Blanco) shows his absent. This may suggest that this transition is not gradual, at least to the south of the study area and can be related to a structural control. Moreover, this transition indicates that the Tacuarembó Formation was uplifted in the eastern area of Otumpa hills. Finally, although some correlations were carried out between stratigraphic units, which most are still informal, and geoelectric layers, the lithology provides more specific scale to analyze the control over the geoelectric layers previously defined.

### Electrical properties, lithology and hydrogeology

The apparent resistivity values of the subsurface are variable due to different factors such as the lithologic type, the presence of fluid, the fluid composition, porosity and permeability of the rock as well as the presence of conductive minerals, among others. General approaches were carried out to constrain these degrees of freedom in order to determinate the hydrogeological features of the study area. In particular, borehole data collected during the field work and a lithologic analysis were added to the geoelectric-stratigraphic analysis performed

in the previous section (see Relations between stratigraphic units and geoelectric layers, Figure 8 and Table 2).

We associated the more conductive geoelectric layers HC and HC<sub>2</sub> (< 5  $\Omega$ m) and C and C<sub>2</sub> (4 to 8  $\Omega$ m), located between 50 and 200 meters, with the presence of high saline water (Figures 5 and 7). The lithology is represented by loess of the Pampa formation, interstratification of sand and pelite sediment of the Chaco formation and outcropping sandstones of the Tacuarembó Formation with an excellent porosity (> 15%). All these rocks can acquire highly conductive electrical values as carriers of high saline waters or clay minerals. In this case, we know that most local groundwater obtained and used has a high saline content and thus a very poor quality. Therefore, the main responsible for the high conductivity modeled was attributed to these water levels. Additional borehole information corroborates the presence of water. The boreholes reach these hydrogeological levels between 80 and 180 meters or even deeper and these depths are in agreement with the location of the high conductive layers. In addition, the conductive layer HC<sub>2</sub> lies between 250 and 350 meters and suggests another potential deeper reservoir (Figures 5 and 7). This water source is consistent with other thermal high saline water found to the southeast, in the Chaco province, at around 350 meters (Coriale, 2006).

On the other hand, the 6 to 20  $\Omega$ m that characterize the SC and SC<sub>2</sub> layers suggest the presence of freshwater (Figures 5 and 7). In the northern area, we associated this geoelectric layers with the Pampa formation, the shallowest unit mainly composed of loess and upper sand units (see Relations between stratigraphic units and geoelectric layers). The subtropical loess in this area is very silty and the upper sand unit has an aeolian origin, so they represent optimum aquifers. In contrast, SC<sub>2</sub> in the southern area is related to sand and pelitic rocks of the Chaco formation and in the eastern area, is related to very porous sandstone of Tacuarembó Formation. There are local water boreholes that reach freshwater between 10 and 70 meters (Rocha-Fasola *et al.*, 2009; Peri, 2012). This hydrogeological level is probably related to SC<sub>2</sub>, whose depths are similar in the VES profile, between 20 and 100 meters and in the northern AMT profile, between 40 and 150 meters (Figures 5 and 7). Also, in the southern AMT profile, SC<sub>2</sub> lies between 80 and 150 meters approximately, which also coincides with freshwater observed in the southern area (Coriale, 2006). However, the saturated thicknesses for both the north and south hydrogeological levels are unknown.

Finally, a very shallow and thin layer around 10 meters thick, which

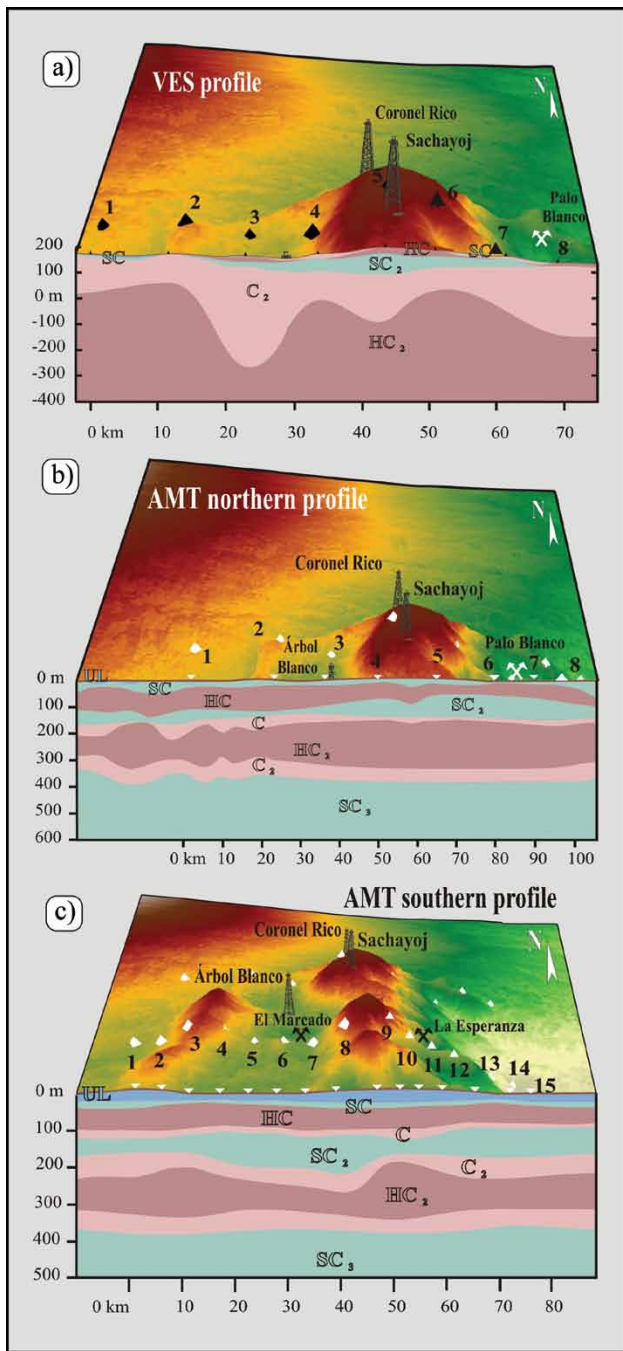


Figure 9. a) A block diagram that combine the 2-D VES model obtained and interpreted and the topography is shown. b and c) Two block-diagrams that combine the 2-D AMT models obtained and interpreted and the topography are shown.

usually hosts freshwater, showed less relevance (Figures 5 and 7). The local boreholes reach this temporary hydrogeological level between one and 15 meters. SC is related to this shallowest water in all profiles. Also, the shallow and constrained UL appears on surfaces associated with salt crusts which are originated by the very arid climate and evaporation.

In summary, the semi-conductive geoelectric layers SC and SC<sub>2</sub> show the best hydrogeological possibilities. SC<sub>2</sub> has a maximum thickness of around 100 meters and shows values that reflect the presence of freshwater. Besides, in the north area, SC<sub>2</sub> provides continuity westward

to a geoelectric layer identified to the east with similar characteristics (Rocha-Fasola *et al.*, 2009). However, the main exploited aquifer in the entire study area must be related to the more conductive geoelectric layers HC (< 5 Ωm) and C (4 to 8 Ωm) in the AMT profile, equivalent to C<sub>2</sub> in the VES profile. This hydrogeological level has high saline content and is 100 meters thick on average.

**Topography, geomorphology and geoelectric layers**

Some geoelectric layers are related to the topography and geomorphology that characterize Otumpa hills. In the VES profile and southern AMT profile, it is clearly observed that HC<sub>2</sub> shows a relief association since it lies in a higher level and is thicker beneath the eastern (between AMT sites 9 and 13 and VES 4 and 7) and western hills (between AMT sites 1 and 4 and VES 1 and 2) and thinner in the lower area between them (between AMT sites 4 and 8 and VES 3) (Figures 9a and 9c). Also, C<sub>2</sub> is thicker in the low area, which is clearly observed around VES 3. The other evidence related to the topography is the gentle tilt to the west of mainly HC, SC<sub>2</sub>, SC, C and HC<sub>2</sub> from the center of the northern AMT profile (AMT site 4) to its west extreme, which is a feature observed in the western slope of Otumpa hills (Figure 9b). In the VES profile, the same gentle tilt is observed from VES 2 to the west (Figure 9a). In both northern profiles, the eastern slope with gentle tilt to the east is reflected from AMT site 6 and VES 6 eastward (Figures 9a and 9b). An unexpected behavior is observed for SC<sub>2</sub>, which becomes thinner in the low area in the southern profile (between AMT sites 4 and 9; Figure 9c) and it moves eastward beneath the highest hill (210 meters), in both northern profiles (between AMT sites 3 and 8 and VES 3 and 7; Figures 9a and 9b). There, it shows lenticular geometry that accompanies the morphostructure and geomorphology. Finally, the undulating surface of HC<sub>2</sub> seems to be related to the uplifted areas (Figure 9).

**Basement control over shallow layers**

Although tectonic stability typifies the study area, it is possible that the shallowest sedimentological units are affected by modern deeper deformation. We counted with previous subsurface information from seismic and gravimetric data that revealed the structure of the basement (crystalline and Paleozoic and Mesozoic units). The main basement structures consist of high angle normal faults and subsequently affected by compressive tectonic regimen (Peri, 2012). Pop-up structures and tilted blocks characterize the deformation of deep subsurface that was transferred to the surface by shallow ductile deformation evidenced by gentle tilt of the more superficial layers.

Our results are in agreement with the deeper structural control of the shallower deformation, which is partially manifested over the local topography. The undulating surfaces of the deepest geoelectric layers (HC<sub>2</sub>, C<sub>2</sub>), geoelectric structures slightly tilted and little vertical displacements seem to reflect a shallow deformation zone (Figure 9). The relevance of define this area resides in the fact that the thickness variations and its subordinated structures could enhance or disturb the lateral and vertical connection between adjacent hydrogeological layers.

**DISCUSSION: HYDROGEOLOGICAL POSSIBILITIES AND CORRELATIONS WITH KNOWN AQUIFER SYSTEMS**

Table 2 summarizes the most significant correlations and properties found of the identified aquifers. Both the shallowest aquifers with semi-conductive geoelectric values (SC-SC<sub>2</sub>) and the deepest one with more conductive geoelectric values (HC-C<sub>2</sub>) could be associated with the Alluvial Fan Aquifer Complex of TAS (Table 2). Particularly, SC<sub>2</sub> could be related to the shallowest aquifer level of this complex because



it has analogous depth, a lenticular shape, good quality water and the same hosted formation (Quaternary units). In addition, the more conductive aquifer could be related to the second deeper level of the Alluvial Fan Aquifer Complex of the TAS.

The mainly hosts of these aquifers are the Pampa and Chaco formations, which eastward becomes the Tacuarembó Formation. This passage led us to conjecture that a transition zone from TAS to GAS occurred to the east. Also, it is worth mentioning that in the north area, both distinctive aquifers lie at similar depths and shows an increase of the conductivity from east to west. This conductivity transition could indicate that it constitutes the same hydrogeological level which varies its composition locally. However, in the south, the semi-conductive layer remains under the conductive layer.

The deep geoelectric layer HC<sub>2</sub> was associated with thermal high saline groundwater. The host sedimentary units for this saline and deep groundwater are the Chaco and Tacuarembó formations. The possible thermal high saline characterization of this aquifer led us to conjecture a closer association with the GAS, which has several thermal manifestations, more than with TAS. Also, this level is related to the topography because it is higher and thicker beneath the hills.

In summary, the study area is placed in a boundary aquifer zone, which suggests an association with both the GAS and the TAS. Essentially, the shallowest levels hosted in Quaternary and Tertiary sediments could be part of the TAS and pass the GAS eastward, for a transition change to the Tacuarembó Formation as host. These shallowest levels involve two aquifers, one containing freshwater and the other containing highly saline water. The deepest hydrogeological level could be related to a thermal aquifer of the GAS.

However, more studies, such as the stable isotopic ratio technique, must be applied to corroborate the origin of these waters. Also, it is essential to carry out more studies to specify the saturated zone of these hydrogeological levels. Finally, we propose exploring the storage capacity of the paleo-channel units which are constituted by unconsolidated sand with excellent porosity and permeability. Currently, the paleo-channels are informally exploited and provide freshwater with very good quality. Although the paleo-channels constitute small, local and temporary aquifers, they constitute an efficient water resource.

## CONCLUSIONS

A shallow geological-geophysical model of the Otumpa hills area was obtained from the application of non-invasive geophysical methods (AMT and VES) in two W-E profiles and constrained by stratigraphical boreholes and field work data. From 1-D and 2-D inversions models, we defined several geoelectric layers that were very consistent between both different methods and profiles. We identified the upper geoelectric layer UL (>20 Ωm), the semi-conductive geoelectric layers SC, SC<sub>2</sub> and SC<sub>3</sub> (6–20 Ωm), the conductive geoelectric layers C and C<sub>2</sub> (4–8 Ωm) and the highly conductive geoelectric layers HC and HC<sub>2</sub> (<5 Ωm).

According with the geoelectric layer features and their distribution, we characterized two main shallow aquifers, one containing freshwater, which is related to semi-conductive geoelectric layers, and the other containing highly saline water, which is related to conductive geoelectric layers.

The semi-conductive geoelectric layers SC and SC<sub>2</sub> present the best properties associated with freshwater possibilities. The shallowest layer SC is about 10 meters thick, whereas SC<sub>2</sub> is about 100 meters thick, but the latter is too variable because of its lenticular geometry. In the north, its host sedimentary unit is the Quaternary Pampa formation, while to the southwest is the Chaco formation. Eastward, the host becomes mainly Chaco and Tacuarembó formations since they are

laterally uplifted. So, SC and SC<sub>2</sub> lie on very porous aeolian sandstone and very silty loess. SC<sub>2</sub> indicates a significant dependence on the relief and geomorphology. In the north area, it provides continuity westward to a geoelectric layer identified to the east with similar characteristics. The saturated zone is unknown but surely very fluctuant since its recharge has a climatic dependence. Several local boreholes corroborate the presence of freshwater at both levels.

On the other hand, the conductive geoelectric layers HC and C in the AMT profiles and C<sub>2</sub> in the VES profile suggest the presence of high saline water. This aquifer is hosted by the Pampa and Chaco formations, with very porous sandstones and very silty loess, and is 100 meters thick on average although more constant than SC<sub>2</sub>. This aquifer is the most exploited in this area. Finally, the deepest aquifer HC<sub>2</sub> could be related to the thermal high saline water from a deep reservoir.

Since the study area is placed in boundary zone aquifer systems, it might be related to both the GAS and the TAS. Essentially, the two shallowest levels hosted in Quaternary and Tertiary sediments could be part of the TAS and pass the GAS eastward, for a transition hosted change to the Tacuarembó Formation. Also, the deepest aquifer could be related to the GAS since the hosts are mainly the Tacuarembó and Chaco formations.

The hydrogeological levels suggest a direct association with the lithology and topography more than with the stratigraphy. Also, some geoelectric layers showed a significant dependence on the relief and geomorphology of Otumpa hills with features such as undulating surfaces, NNE-SSW trend of some levels, lenticular geometries and gentle tilts that accompany the slopes in the same directions.

Finally, the relevance of this work resides in the fact that the water resources in this region are scarce and usually poorly managed. The results not only allow defining and planning locally the aquifers reservoirs but also allow focusing into regional research. Moreover, the results obtained led us to consider that will be necessary obtain more measurement sites that allow us to improve the lateral resolution in the future. So, further studies are likely to provide new insights into the hydrological interaction between two significant Guaraní and Yrendá-Toba-Tarijeño aquifer systems of the South American region.

## ACKNOWLEDGMENTS

We thank the Argentine Council for Scientific and Technical Research (CONICET, grant PIP D703, 2011) and the University of Buenos Aires (UBACYT, EX 272 and X194) for providing financial support to improve the logistics. We also thank Gabriel Giordanengo (Instituto de Geocronología y Geología Isotópica, INGEIS, Buenos Aires) for his valuable technical assistance during the surveys and our colleagues Oscar Coriale (Instituto Nacional del Agua, INA, Buenos Aires), Verónica Rocha-Fasola (CONHIDRO, Salta), Dr. Hugo Marengo (Servicio Geológico Minero Argentino, SEGEMAR, Mendoza) and Dr. Griselda Galindo (Universidad de Buenos Aires, UBA), who contributed valuable information for this work.

## REFERENCES

- Angeleri, J.L., 2002, Estudio de Aprovechamiento de Acuíferos en el oeste de la Región Chaqueña Argentina (on line): < <http://www.unsa.edu.ar/inasla/tat/download/chaco/>>, 12 pp.
- Araújo, L.M., França, A.B., Potter, P.E., 1995, Aquífero Gigante do Mercosul no Brasil, Argentina, Uruguai e Paraguai, Mapas Hidrogeológicos das Formações Botucatu, Pirambóia, Rosário do Sul, Buena Vista, Misiones e Tacuarembó. Mapas: Curitiba, Brazil, UFPR-Petrobras, Technical report, 16 pp.

- Araújo, L.M., França, A.B., Potter, P.E., 1999, Hydrogeology of the Mercosul aquifer system in the Paraná and Chaco Paraná Basins, South America, and comparison with the Navajo-Nugget aquifer system, USA: *Hydrogeology Journal*, 7 (3), 317-336.
- Bahr, K., 1988, Interpretation of the magnetotelluric impedance tensor: regional induction and local telluric distortion: *Journal of Geophysics*, 62, 119-127.
- Bahr, K., 1991, Geological noise in magnetotelluric data: a classification of distortion types, *Physics of the Earth and Planetary Interiors*, 66 (1-2), 24-38.
- Batic, O., Cortelezzi, C., Pavlicevic, R., Traversa, L., 1995, Caracterización tecnológica de las areniscas cementadas con calcedonia y ópalo del noroeste de la Provincia de Chaco, in 12th Reunión Técnica de la Asociación Argentina Tecnológica del Hormigón, La Plata, Argentina: La Plata, Argentina, 191-196.
- Baudino, G. A., Pitzzu, G., Bercheñi, G., Bercheñi, V., Fuertes, A., Mandjarres, C., 2006, Estudio Hidrogeológico en la porción apical del abanico aluvial del río Pilcomayo, entre Ibibobo y Misión La Paz/Pozo Hondo, 2ª etapa Correlación Hidroestratigráfica: Salta, Argentina, Convenio Proyecto de Gestión Integrada y Plan Maestro del río Pilcomayo - Universidad Nacional de Salta, Technical report, 52 pp.
- Berdichevsky, M.N., Dmitriev, V.I., 2008, *Models and Methods of Magnetotellurics*, first edition: Berlin, Germany, Springer-Verlag, 563 pp.
- Bobachev, A., Modin I., Shevnev, V., 2011, IPI2WIN, 1D interpretation of VES profile, version 3.1.2c: Moscow, Russia, Moscow State University, software.
- Bonini, L., 1980, Prospección Geoelectrica en el yacimiento cuarcítico Palo Blanco, Provincia del Chaco: Buenos Aires, Argentina, Instituto Nacional de Ciencia y Técnica Hídricas, Centro de hidrología Aplicada, Unidad Geofísica, Technical report, 22 pp.
- Bossi, J., 1966, Geología del Uruguay: Montevideo, Uruguay, Departamento de Publicaciones de la Universidad de la República: Science collection, 2, 464 pp.
- Castellanos, A., 1968, Desplazamientos naturales, en abanico, del río Salado del Norte en la llanura Chaco-Santiaguense-Santafesina: Rosario, Argentina, Instituto de Fisiografía y Geología: Universidad Nacional de Rosario, Scientific report, 52, 19 pp.
- Chebli, G.A., Tofalo, O., Turzzini, G.E., 1989, Mesopotamia, in Chebli, G.A., Spaletti L.A. (eds.) *Cuencas Sedimentarias Argentinas: Tucumán, Argentina: Serie Correlación Geológica*, Instituto Superior de Correlación Geológica, Universidad Nacional de Tucumán, 6, 79-100.
- Chebli, G., Mozetic, M., Rossello, E., Bühler, M., 1999, Cuencas sedimentarias de la llanura Chacopampeana, in Caminos, R. (ed.), *Geología Argentina anales 29 (20)*: Buenos Aires, Instituto de Geología y Recursos Minerales, 627-644.
- Constable, S.C., Parker, R.L., Constable, C.G., 1987, Occam's inversion: a practical algorithm for generating smooth models from electromagnetic sounding data: *Geophysics*, 52, 289-300.
- Coriale, O., 2006, Estudio de fuentes de agua subterránea con fines de provisión de agua potable y exploración hidrotermal: Ezeiza, Buenos Aires, Instituto Nacional del Agua (INA), Technical report, 104 pp.
- De Santa Ana, H., Verloslabsky, G., Fúlfaro, V.J., Fernández-Garrasino, C.A., 2008, Síntesis sobre la geología regional del Sistema Acuífero Guaraní - Informe Técnico PSAG: Montevideo, Uruguay, Proyecto para a Protecao Ambiental e Desenvolvimento Sustentável do Sistema Acuífero Guaraní, Technical report, 155 pp.
- Dirección General de Minas y Geología (DGMG), 1947, Perforación hidrogeológica N°1 en la localidad de Sachayoj, Provincia de Santiago del Estero: Buenos Aires, Argentina, Dirección General de Minas y Geología (DGMG), Technical report, 2 pp.
- Falgàs, E., 2007, Hydrogeophysics as a multidisciplinary tool on aquifer appraisal: focus on AMT capabilities: Spain, Universidad de Barcelona, Ph.D. Thesis, 208 pp.
- Fernández-Garrasino, C., Laffitte, G., Villar, H., 2005, Cuenca Chacoparanaense, in Chebli, G.A., Cortiñas, J.S., Spalletti, L.A., Legarreta, L., Vallejo, E.L. (eds.), 6º Congreso de Exploración y Desarrollo de Hidrocarburos, Frontera Exploratoria de la Argentina, Mar del Plata, Argentina, Proceedings, 97-114.
- Fuertes, A., 2004, Caso de estudio Sistema Acuífero Yrendá-Toba-Tarijeño-Paraguay-Argentina-Bolivia: Salta, Argentina, Programa marco para la gestión sostenible de los recursos hídricos de la Cuenca del Plata en relación con los efectos hidrogeológicos de la variabilidad y el cambio climático, Technical report, 41 pp.
- Gastmans, D., Chang, H.K., Hutcheon, I., 2010, Groundwater geochemical evolution in the northern portion of the Guaraní Aquifer System (Brazil) and its relationship to diagenetic features: *Applied Geochemistry*, 25 (1), 16-33.
- Gastmans, D., Veroslavsky, G., Kiang Chang, H., Caetano-Chang, M. R., Nogueira Pressinotti, M. M., 2012, Modelo hidrogeológico conceptual del Sistema Acuífero Guaraní (SAG): una herramienta para la gestión: *Boletín Geológico y Minero*, 123 (3), 249-265.
- Groom, R.W., Bailey, R.C., 1989, Decomposition of magnetotelluric impedance tensors in presence of local three-dimensional galvanic distortion: *Journal of Geophysical Research*, 94 (B2), 1913-1925.
- Iriondo, M.H., 1984, The Quaternary of Northeastern Argentina, in Rabassa, J. (ed.), *Quaternary South American and Antarctic Peninsula*, 2: Rotterdam, Netherlands, 51-78.
- Iriondo, M.H., 1990, La Formación Urundel, un loess chaqueño, in *International Symposium on Loess: Mar del Plata, Argentina*, International Union for Quaternary Research (INQUA), Abstracts, 89-90.
- Iriondo, M.H., 1993, Geomorphology and late Quaternary of the Chaco (South America): *Geomorphology*, 7, 289-303.
- Iriondo, M.H., 1997, Models of deposition of loess and loessoids in the Upper Quaternary of South America: *Journal the South American Earth Sciences*, 10 (1), 71-79.
- Iriondo, M.H., Bautista, J.A., 2008, El Cuaternario de Bolivia y regiones vecinas: Santa Fe, Argentina, Museo Provincial de Ciencias Naturales Florentino Ameghino, 378 pp.
- Iriondo, M., García, N., 1993, Climatic variations in the Argentine plains during the last 18,000 years: *Palaeogeography, Paleoclimatology, Palaeoecology*, 101, 209-220.
- Kaufman, A.A., Keller, G.V., 1981, *The Magnetotelluric Sounding Method*: Amsterdam, Elsevier, 595 pp.
- LaTorraca, G. A., Madden, T. R., Korringa, J., 1986, An analysis of the magnetotelluric impedance for three-dimensional conductivity structures: *Geophysics*, 51, 1819-1829.
- Marengo, H.G., 2006, *Micropaleontología y estratigrafía del Mioceno marino de la Argentina: Las Transgresiones de Laguna Paiva y del "Entrerriense-Paranense"*: Buenos Aires, Argentina, Universidad de Buenos Aires, Departamento de Geología, PhD Thesis, 124 pp.
- McNeill, J., 1990, Use of electromagnetic methods for groundwater studies: *Geotechnical and Environmental Geophysics*, Oklahoma, 1, 191-218.
- Mon, R., Gutiérrez, A.A., 2009, The Mar Chiquita Lake: An indicator of intraplate deformation in the central plain of Argentina: *Geomorphology*, 111, 111-122.
- Orellana, E., 1972, *Prospección Geoelectrica en Corriente Continua*: Madrid, España, Editorial Paraninfo, 532 pp.
- Padula, E., Mingramm, A., 1963, The fundamental geological pattern of the Chaco-Paraná Basin (Argentina) in relation to its oil possibilities, in 6th World Petroleum Congress, Frankfurt, Germany, Section 1, 293-310.
- Pasotti, P., 1968, Evidencias morfológicas del levantamiento de la "Pampa Levantada" en un sector de la llanura Santafesino-Bonaerense: Rosario, Argentina, Instituto de Fisiografía y Geología, Universidad Nacional de Rosario, Scientific report, 53, 46 pp.
- Pasotti, P., 1974, *La Neotectónica en la Llanura Pampeana. Fundamentos para el mapa neotectónico*: Rosario, Argentina, Instituto de Fisiografía y Geología, Universidad Nacional de Rosario, Scientific report, 58, 27pp.
- Peri, V.G., 2012, Caracterización morfoestructónica de las Lomas de Otumpa (Gran Chaco, Santiago del Estero y Chaco): influencias en el control del drenaje: Buenos Aires, Argentina, Facultad de Ciencias Exactas y Naturales, Universidad Nacional de Buenos Aires, PhD Thesis, 321 pp.
- Peri, V.G., Rossello, E.A., 2010, Anomalías morfoestructurales del drenaje del río Salado sobre las Lomas de Otumpa (Santiago del Estero y Chaco) detectadas por procesamiento digital: *Revista de la Asociación Geológica Argentina*, 66(4), 636-648.
- Pezzi, E.E., Mozetic, M.E., 1989, Cuencas Sedimentarias de la región Chacoparanaense, in Chebli, G.A., Spaletti, L.A. (eds.), *Cuencas Sedimentarias Argentinas, Serie Correlación Geológica 6: Tucumán, Argentina*, Instituto Superior de Correlación Geológica (INSUGEO), 65-78.

- Ramos-Leal, J.A., López-Loera, H., Martínez Ruiz, V.J., Aranda-Gómez, J.J., 2007, Sucesión de eventos y geometría de la parte central del acuífero del graben de Villa de Reyes (San Luis Potosí, México) inferida a partir de datos geoelectrónicos: *Revista Mexicana de Ciencias Geológicas*, 24 (1), 31-46.
- Reddy, I.K., Rankin, D., Phillips, R.J., 1977, Three dimensional modelling in magnetotelluric and magnetic variation sounding: *Geophysical Journal of the Royal Astronomical Society*, 5(3), 13-325.
- Rocha-Fasola, V., García Ortiz M.F., Martínez, C. A., 2009, Estudios hidrogeológicos para la exploración de agua subterránea en la Provincia del Chaco. Zona Sudoeste, Área Charata-Avia Terai, Provincia de Chaco: Salta, Argentina, Empresa de Construcciones e Hidrología - CONHIDRO LTDA, Technical report, 34 pp.
- Rodi, W., Mackie, R.L., 2001, Nonlinear conjugate gradients algorithm for 2D magnetotelluric inversion: *Geophysics*, 66 (1), 174-187.
- Rossello, E.A., Bordarampé, C.P., 2005. Las Lomadas de Otumpa: nuevas evidencias cartográficas de deformación neotectónica en el Gran Chaco (Santiago del Estero, Argentina), *in* 16th Congreso Geológico Argentino, La Plata, Buenos Aires, CD-ROM, Paper N° 210.
- Rossello, E. A., Veroslavsky, G., 2012, Definición del límite occidental del Sistema Acuífero Guaraní (Gran Chaco, Argentina): ¿técnico o convencional?: *Boletín Geológico y Minero*, 123 (3), 297-310.
- Russo, A., Ferello, R., Chebli, G., 1979, Llanura Chaco-Pampeana, *in* 2° Simposio de Geología Regional Argentina, Córdoba, Argentina, Volume I, 139-183.
- Sayago, M., Collantes, M.M., Karlson, A., Sanabria, J., 2001, Genesis and distribution of the Late Pleistocene and Holocene loess of Argentina: a regional approximation: *Quaternary International*, 76/77, 247-257.
- Scherer, C.M., 2002, Preservation of aeolian genetic units by lava flows in the Lower Cretaceous of the Paraná Basin, southern Brazil: *Sedimentology*, 49, 97-116.
- Simpson, F., Bahr, K., 2005, *Practical Magnetotellurics*: Cambridge University press, first ed., 254 pp.
- Swift, C., 1967, A magnetotelluric investigation of an electrical conductivity anomaly in the southwestern United States: Cambridge, England, MIT Press. Cambridge, PhD Thesis, 211 pp.
- Vargas, R., 1977, Soluciones al Problema de Agua en la Expansión de la Frontera Agropecuaria de la Provincia del Chaco: Resistencia, Chaco, Argentina, Campaña del Oeste - Programa III - Estudio Hidrogeológico Pico del Chaco, Technical report, 45 pp.
- Vives, L., Campos, H., Candela, L., Guarracino, L. 2001, Modelación del acuífero Guaraní: *Boletín Geológico y Minero*, 112, 51-64.
- Volponi, F., Aparicio, E., 1969, La Actividad en las zonas mesosísmicas del territorio argentino: *Anales de la Sociedad Científica Argentina*, 184, Series I, Ciencias 12, 49-58.
- Vozzoff, K., 1972, The magnetotelluric method in the exploration of sedimentary basins: *Geophysics*, 37, 98-141.
- Wiens, F., 1995, Phanerozoic tectonics and sedimentation in the Chaco Basin of Paraguay, with comments on hydrocarbon potential, *in* Tankard, A.J., Suárez, S.R., Welsink, H.J. (eds.), *Petroleum Basins of South America*: Tulsa, United States of America, American Association of Petroleum Geologists Memoir, 62, 185-205.
- Yacimientos Petrolíferos Fiscales (YPF), 1943, Informe Técnico de la Perforación petrolera Charata (YPF.CH.1): Buenos Aires, Argentina, Yacimientos Petrolíferos Fiscales (YPF), Technical report, 37 pp.
- Yacimientos Petrolíferos Fiscales (YPF), 1966a, Informe Técnico de la Perforación petrolera Alhuampa (DGMG): Buenos Aires, Argentina, Yacimientos Petrolíferos Fiscales (YPF), Technical report, 23 pp.
- Yacimientos Petrolíferos Fiscales (YPF), 1966b, Informe Técnico de la Perforación petrolera Árbol Blanco (YPF.SE.AB.x-1): Buenos Aires, Argentina, Yacimientos Petrolíferos Fiscales (YPF), Technical report, 32 pp.
- Yacimientos Petrolíferos Fiscales (YPF), 1969a, Informe Técnico de la Perforación petrolera Campo Gallo (YPF.SE.CG.x-1): Buenos Aires, Argentina, Yacimientos Petrolíferos Fiscales (YPF), Technical report, 45 pp.
- Yacimientos Petrolíferos Fiscales (YPF), 1969b, Informe Técnico de la Perforación Petrolera Coronel Rico (YPF.SE.CR.x-1): Buenos Aires, Argentina, Yacimientos Petrolíferos Fiscales (YPF), Technical report, 56 pp.
- Yacimientos Petrolíferos Fiscales (YPF), 1970, Informe Técnico de la Perforación petrolera Gancedo (YPF.Cha.G.x-1): Buenos Aires, Argentina, Yacimientos Petrolíferos Fiscales (YPF), Technical report, 21 pp.
- Zonge, K.L., Hughes, L.J., 1988, Controlled source audio-frequency magnetotellurics, *in* Nabighian, M.N. (ed.), *Electromagnetic methods in Applied Geophysics- theory and practice*: Tulsa, United States of America, Society of Exploration Geophysicists, 2, 713-809.

Manuscript received: May 6, 2013

Corrected manuscript received: September 6, 2013

Manuscript accepted: September 9, 2013